# Static and dynamic spin correlations in pure and doped $La_2CuO_4$

Y. Endoh and K. Yamada
*Department of Physics, Tohoku University, Sendai 980, Japan*

R. J. Birgeneau, D. R. Gabbe, H. P. Jenssen, M. A. Kastner, C. J. Peters, P. J. Picone, and T. R. Thurston
*Center for Materials Science and Engineering, Massachusetts Institute of Technology, Cambridge, Massachusetts 02139*

J. M. Tranquada and G. Shirane
*Physics Department, Brookhaven National Laboratory, Upton, New York 11973*

Y. Hidaka, M. Oda, Y. Enomoto, M. Suzuki, and T. Murakami
*Nippon Telegraph and Telephone Electrical Communications Laboratories, Tokai, Ibaraki 319-11, Japan*
(Received 28 December 1987)

We report elastic, quasielastic ($\int dE$), and inelastic neutron-scattering studies of the instantaneous and dynamic spin fluctuations in as-grown and doped $La_2CuO_4$. Four samples have been studied: (A) as-grown $La_2CuO_4$ with $T_N = 195$ K, (B) oxygenated $La_2CuO_4$ with $T_N \simeq 100$ K, (C) $La_2Cu_{0.95}Li_{0.05}O_4$, and (D) $La_{1.97}Sr_{0.03}Cu_{0.95}Li_{0.05}O_4$. All crystals exhibit variable-range-hopping conductivity behavior. At room temperature each sample exhibits two-dimensional (2D) antiferromagnetic instantaneous correlations in the $CuO_2$ sheets with the correlation length varying from $\sim 200$ Å in crystal A to $\sim 14$ Å in crystal D. The integrated intensity and therefore the effective moment is, however, constant to within the experimental error. In samples A and B the 2D correlation length becomes sufficiently large with decreasing temperature that the interplanar coupling is able to derive a transition to 3D long-range order. The spin dynamics have been studied in detail in crystals A and B and quite unusual behavior is observed. In contrast to previously studied planar antiferromagnets, there is no significant $E \simeq 0$ component for temperatures $\geq T_N$ and instead the 2D response function is highly inelastic. The effective dispersion of the spin excitations is $\geq 0.4$ eV Å. This large energy scale for the spin fluctuations gives credence to models of the superconductivity in doped $La_2CuO_4$ in which the pairing is magnetic in origin.

## I. INTRODUCTION

The discovery of superconductivity in doped $La_2CuO_4$ by Bednorz and Müller[1] has stimulated an enormous number of experimental and theoretical studies of this and related materials. It is broadly viewed that in order to understand the novel high-temperature superconductivity, it will be necessary to elucidate fully the behavior across the phase diagram as a function of temperature, doping, etc. It is already known that the phase diagram is remarkably rich with competing or attendant phases and phase transitions including a tetragonal-orthorhombic structural transition,[2-5] three-dimensional (3D) antiferromagnetic ordering,[6,7] a crossover from a 3D Néel to a 2D quantum spin fluid state[8] and possibly a low-temperature 3D spin-glass state,[8-11] an insulator-metal transition,[5,12] and, of course, the superconducting transition.[1,4]

In any model for the superconductivity, the spin-degrees of freedom of the $Cu^{2+}$ ions are essential and, indeed, in many models, the magnetism is the progenitor of the high-temperature superconductivity.[11,13] It is therefore essential that the microscopic static and dynamic spin fluctuations in both pure and doped $La_2CuO_4$ be elucidated in detail. Such experiments can only be done properly utilizing large, high quality homogeneous single crystals and thus these measurements place great demands on crystal-growth techniques.[3,14,15] In this paper we report the results of a detailed neutron scattering study of the spin fluctuations in four crystals: (A) as-grown $La_2CuO_4$, (B) oxygenated $La_2CuO_4$, (C) $La_2Cu_{0.95}Li_{0.05}O_4$, and (D) $La_{0.97}Sr_{0.03}Cu_{0.95}Li_{0.05}O_4$. The first two crystals were grown at Nippon Telegraph and Telephone (NTT) Electrical Communications Laboratories[15] and the latter two at Massachusetts Institute of Technology[14] (MIT). Preliminary results on crystal A were reported in Ref. 8.

The format of this paper is as follows. In Sec. II the crystal and 3D magnetic structures of $La_2CuO_4$ are discussed; we also review the bulk magnetic properties of the pure and doped materials. A brief discussion of the crystal growth and characterization is also given. Quasielastic measurements of the instantaneous two-dimensional correlations are presented in Sec. III. The magnetic inelastic scattering measurements are reported in Sec. IV. Some limited polarized neutron data are given in Sec. V. Finally, in Sec. VI we present a discussion of the results

 

with emphasis on their relationship to current theories and their implications for the high-temperature superconductivity in doped $La_2CuO_4$.

## II. PRELIMINARY DETAILS

The crystal and magnetic structures of $La_2CuO_4$ are shown in Fig. 1. At high temperatures $La_2CuO_4$ has the $K_2NiF_4$ crystal structure;[16] below $\sim$500 K the system undergoes a tetragonal-to-orthorhombic structural transition[2,3,17] which involves primarily a staggered rotation of the $CuO_6$ octahedra as illustrated in Fig. 1; the rotations are uniform in a given **a**-**b** plane. The space group in the orthorhombic phase is *Cmca*. Stoichiometric $La_2CuO_4$ orders antiferromagnetically at $\sim$300 K with the magnetic structure shown in Fig. 1.[6,7] The structure is characterized first by a simple 2D antiferromagnetic array in the $CuO_2$ planes with nearest neighbors antiparallel; the spins are in the **b**-**c** plane canted 0.17° away from the **c** axis (Thio *et al.*, Ref. 7). The orthorhombic distortion lifts the frustration of the magnetic interactions between neighboring $CuO_2$ planes so that a unique 3D ordering pattern is established. Specifically, as shown in Fig. 1, the $Cu^{2+}$ spins are aligned ferromagnetically in **b**-**c** planes. Since $|a| < |c|$ this suggests that the between-plane coupling is antiferromagnetic. The 3D ordering temperature is remarkably sensitive to doping.[10,18,19] The addition of a few percent or less of $Li^+$, $Sr^{2+}$, or $O_2$ destroys the 3D ordering completely. One of the purposes of this research is to elucidate the underlying mechanism for this extraordinary sensitivity of $T_N$ to the concentration of holes.

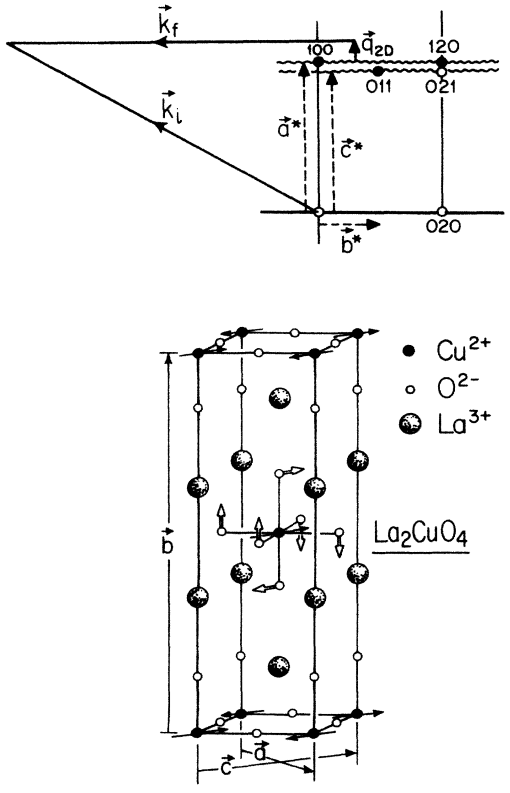


FIG. 1. Top: superposition of **a***-**b*** and **c***-**b*** reciprocal-lattice planes of $La_2CuO_4$ together with a representative scattering diagram for $E=13.7$ meV neutrons. Bottom: crystal and magnetic structure of $La_2CuO_4$; the arrows associated with the center oxygens indicate the direction of rotation in the orthorhombic phase.

As noted in Sec. I, we have studied four crystals in all, two grown at NTT and two at MIT. The NTT crystals were grown using a copper oxide flux method which is extensively described in a recent publication.[15] Both crystals were about 0.5 $cm^3$ in volume. The first, which we label NTT-2, is as-grown. The second, labeled NTT-3, was annealed under flowing $O_2$ gas first at 800 °C for 50 h and then at 550 °C also for 50 h. The MIT crystals were grown using a $Li_4B_2O_5$ flux technique.[14] One, which has no deliberate dopant, corresponds to $La_2Cu_{0.95}Li_{0.05}O_4$, that is, about 5% of the $Cu^{2+}$ is replaced by $Li^+$.[20] This crystal is labeled MIT-2. For the last crystal, the melt contained about 20% $SrCO_3$; this yielded a crystal with approximate stoichiometry $La_{1.97}Sr_{0.03}Cu_{0.95}Li_{0.05}O_4$; this crystal is labeled MIT-1. The lattice constants, tetragonal-to-orthorhombic structural phase transition temperatures $T_{st}$, and 3D magnetic transition temperatures are listed in Table I. The anticipated trends with dopant concentration are indeed observed. Each of these four crystals exhibits variable-range hopping (VRH) conductivity behavior (Refs. 3, 12, 21, and 22), $\sigma \sim \exp[-(T_0/T)^{1/4}]$. We note that $O_2$ treatment causes $La_2CuO_4$ ceramics to become superconducting;[12,23] however, single crystals which are annealed in pressurized oxygen show no evidence of bulk superconductivity. We also confirmed that the soft phonon behavior[3] accompanying the tetragonal-to-orthorhombic transition was closely similar in each of the four crystals.

Before discussing the measurements, it will prove useful to review the various correlation functions measured in magnetic neutron scattering experiments.[24] Generally, one has

$$\frac{\partial^2\sigma}{\partial\Omega_f \partial E_f} \sim \sum_\alpha (1-\hat{Q}_\alpha^2) S^{\alpha\alpha}(\mathbf{Q},\omega) \ , \tag{1}$$

where

$$S^{\alpha\alpha}(\mathbf{Q},\omega) = \frac{1}{2\pi N} \int_{-\infty}^{\infty} e^{-i\omega t} \langle S^\alpha(-\mathbf{Q},0) S^\alpha(\mathbf{Q},t) \rangle dt \ , \tag{2}$$

and

$$\mathbf{S}(\mathbf{Q},t) = \sum_{\mathbf{R}} e^{i\mathbf{Q}\cdot\mathbf{R}} \mathbf{S}(\mathbf{R},t) \ . \tag{3}$$

Here $\mathbf{Q}=\mathbf{k}_i-\mathbf{k}_f$ where $\mathbf{k}_i$ and $\mathbf{k}_f$ are the incoming and outgoing neutron wave vectors, respectively. In an experi-

TABLE I. Crystal parameters.

| Label | Relative volume | $T_{st}$ (K) | $T_N$ (K) | $a$ (Å) | $b$ (Å) | $c$ (Å) |
|---|---|---|---|---|---|---|
| NTT-2 | 1 | 503 | 195 | 5.339 | 13.100 | 5.422 |
| NTT-3 | 1 | 499 | 100 | 5.333 | 13.095 | 5.419 |
| MIT-2 | 0.22 | 423 | | 5.333 | 13.098 | 5.384 |
| MIT-1 | 0.31 | 350 | | 5.323 | 13.084 | 5.379 |

ment in which one integrates over the energy at fixed Q, one measures the *instantaneous* correlation function

$$S^{aa}(\mathbf{Q}) = \int d\omega S^{aa}(\mathbf{Q},\omega) = \frac{1}{N}\langle S^a(-\mathbf{Q},0)S^a(\mathbf{Q},0)\rangle \ . \quad (4)$$

As we shall discuss extensively in Sec. III, because of the large energy scale for the magnetic fluctuations in $La_2CuO_4$, the experimental scattering geometry must be chosen carefully in order to carry out the energy integration in Eq. (4) properly.[25,26] For a system with long-range order (LRO) the Bragg scattering is given by the $\omega = 0$ response in Eq. (1), that is,

$$\left.\frac{\partial^2\sigma}{\partial\Omega_f \partial E_f}\right|_{\text{Bragg}} = \sum_\alpha (1-\hat{G}_\alpha^2)\frac{1}{iN}\langle S^\alpha(\mathbf{G},t)\rangle^2\delta(\omega) \ , \quad (5)$$

where G is a magnetic reciprocal-lattice vector. The directional term $(1-\hat{G}_\alpha^2)$ enables one to determine the ordered spin direction.

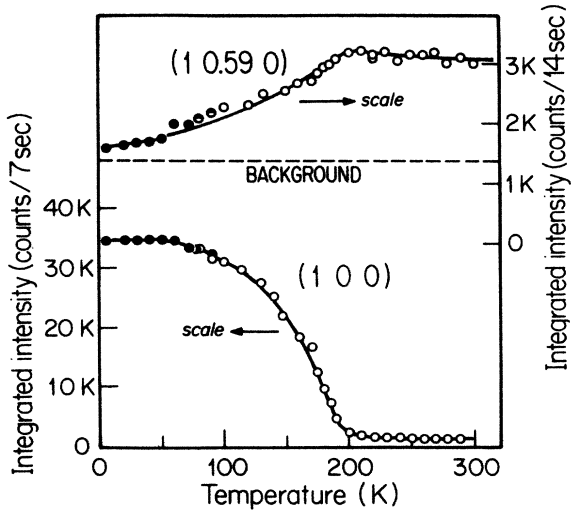


FIG. 2. Integrated intensities of the (100) 3D antiferromagnetic Bragg peak and the (1 0.59 0) 2D rod in NTT-2. The open and closed circles represent separate experiments which were normalized in the overlap region.

## III. ELASTIC AND QUASIELASTIC NEUTRON SCATTERING MEASUREMENTS

### A. 3D Bragg scattering

The neutron-scattering measurements were carried out using the triple-axis spectrometers H7 and H4M at the Brookhaven high-flux beam reactor; for strictly elastic scans ($E \simeq 0$) we use a triple-axis spectrometer set for zero energy transfer and with pyrolitic graphite filters before and after the sample. The samples were mounted either in ovens or in displex or flow cryostats depending on the temperature range being covered. For most of the elastic measurements the neutron energy was 13.7 meV although this energy was often varied in order to minimize multiple-scattering effects; the latter are quite problematic in these crystals in part because of scattering between twin domains. These two-domain double scattering processes violate the *Cmca* extinction rules and thus can be confused with the magnetic scattering.

For all of the measurements the crystals were oriented with an $\mathbf{a}^*$ or $\mathbf{c}^*$ axis vertical; because of twinning, a given tetragonal [110] axis may become either an a or c axis in the orthorhombic phase. Thus the experiments were effectively carried out in a superposition of the $\mathbf{a}^*$-$\mathbf{b}^*$ and $\mathbf{c}^*$-$\mathbf{b}^*$ reciprocal lattice planes. This did not present any special difficulties and indeed, since $\mathbf{a}^*$ and $\mathbf{c}^*$ are easily separated, it often represented an advantage. The allowed nuclear and magnetic reciprocal-lattice points are shown at the top of Fig. 1. Our measurements confirm the magnetic structure proposed by Vaknin *et al.*[6]

The (100) magnetic Bragg intensity for NTT-2 and NTT-3 are shown in the bottom panels of Figs. 2 and 3, respectively. NTT-2 exhibits conventional behavior with $T_N = 195$ K although the transition is rounded by $\sim 5$ K, presumably due to macroscopic inhomogeneities. One important feature is that the order parameter curve for NTT-2 is characteristically 3D in shape compared with say $K_2NiF_4$ which shows clear 2D Ising critical behavior.[6]

We estimate roughly that the saturated moment is $\sim 0.35\mu_B$. The transition for the oxygenated crystal, NTT-3, is, however, much more rounded with a long tail extending to high temperatures. The median Néel temperature is about 100 K. The most dramatic feature evident in Fig. 3 is that the sublattice magnetization $M_S$ in NTT-3 is *reentrant*, that is, it decreases below 25 K. As we shall discuss later, the diminution in $M_S$ below 25 K is accompanied by the appearance of intense 2D $E \simeq 0$ scattering. This is analogous to the reentrant spin-glass behavior seen in 3D systems such as $Eu_xSr_{1-x}S$.[27]

Neither MIT-1 nor MIT-2 exhibits a 3D magnetic transition. Extensive measurements in MIT-2 did show some extra scattering at the (100) position below 130 K but this scattering was at least two orders of magnitude

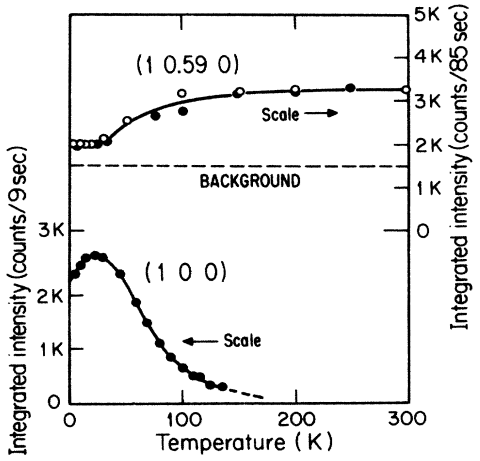


FIG. 3. Integrated intensities of the (100) 3D antiferromagnetic Bragg peak and the (1 0.59 0) 2D rod in NTT-3. The open and closed circles represent separate experiments.

weaker in intensity than the magnetic Bragg scattering discussed above. We have not identified unambiguously the source of this very weak scattering. We conclude, therefore, that the $Li^+$ impurities destroy the 3D magnetic state. As discussed by Kastner *et al.*,[12] 0.05 $Li^+$ also destroys the superconducting state in $La_{1.8}Ba_{0.2}Cu_{0.95}Li_{0.05}O_4$ ceramics. As we shall discuss later, the underlying physics for the deleterious effects in the two cases is quite different.

### B. 2D diffuse scattering

In general, antiferromagnetic transitions in 2D or 3D are accompanied by low-energy, long-distance critical fluctuations.[24,25] In lamellar systems such as $K_2NiF_4$, these low-energy fluctuations are primarily 2D in character.[25,26] Accordingly, we first used a triple-axis spectrometer set for $E=0$ to search for scattering from the anticipated critical fluctuations. However, these measurements revealed neither 3D nor 2D critical fluctuation effects. This is in marked contrast to the behavior seen in all previously studied 2D and 3D antiferromagnets.[26]

Because of the unique nature of the 2D $S=\frac{1}{2}$ Heisenberg antiferromagnet[28] and because of previous experience with corresponding 1D systems,[29] we conjectured that the fluctuations in $La_2CuO_4$ could have anomalous dynamical character. Thus, in an attempt to locate the anticipated 2D fluctuations we changed to a two-axis configuration so that only the outgoing neutron direction but not the energy was fixed. As discussed above in the context of Eq. (7), if the energy intergration is carried out correctly at fixed **Q**, one measures the instantaneous response function $S^{\alpha\alpha}(\mathbf{Q})$. It was discovered in the original critical scattering experiments[25] in $K_2NiF_4$ that this energy integration may be carried out rather elegantly in 2D systems. The appropriate geometry is shown at the top of Fig. 1. If the outgoing neutron wave vector $\mathbf{k}_f$ is along $-\mathbf{b}^*$, that is, perpendicular to the $CuO_2$ sheets, then the in-plane momentum transfer $\mathbf{Q}_{2D}$ is a constant independent of the magnitude of $\mathbf{k}_f$. If all such neutrons are detected than one integrates over $E$ from $-E(\text{cutoff})$ to $\hbar^2 k_i^2/2m$ where $E(\text{cutoff})$ is determined by the $Cu^{2+}$ form factor. For these experiments $-E(\text{cutoff}) \simeq -70$ meV which is much larger than thermal energy at room temperature and therefore is essentially infinite.

We show in Fig. 4 both two-axis and three-axis scans at 200 K in NTT-2; these measurements utilized neutrons of energy 13.7 meV and the spectrometer had collimation 40′-10′-10′-(40′). At (100), 3D magnetic Bragg scattering is observed; the 3D Bragg peak is still present at 200 K because of the rounding of the transition. For both the energy integrating (two-axis) and $\omega=0$ (three-axis) measurements a sharp resolution-limited peak is observed at (100). The difference in intensity of the two-axis and three-axis scans evident in Fig. 4 is due to the 70% reflectivity of the graphite analyzer. Quite different behavior occurs for scans across the 2D rods; for $k_i=2.57$ Å$^{-1}$, a simple calculation gives $\mathbf{k}_f \| -\mathbf{b}^*$ when $\mathbf{Q}_\perp=0.59\mathbf{b}^*$. For the two-axis scan along the in-plane wave vector $\mathbf{Q}_{2D}$ with $\mathbf{Q}_\perp=0.59\mathbf{b}^*$ a flat-top peak with very sharp edges is observed. This flat-top peak is actually a superposition of the $(1\zeta 0)$ and $(0\zeta 1)$ rods of scattering (cf. Fig. 1, top) which are slightly separated in $Q$ as a result of the orthorhombic distortion. In this case, however, hardly any signal occurs in the three-axis scan. Thus, the response function comes overwhelmingly from fluctuations which are at energies much greater than the three-axis energy window of $\simeq 1$ meV.

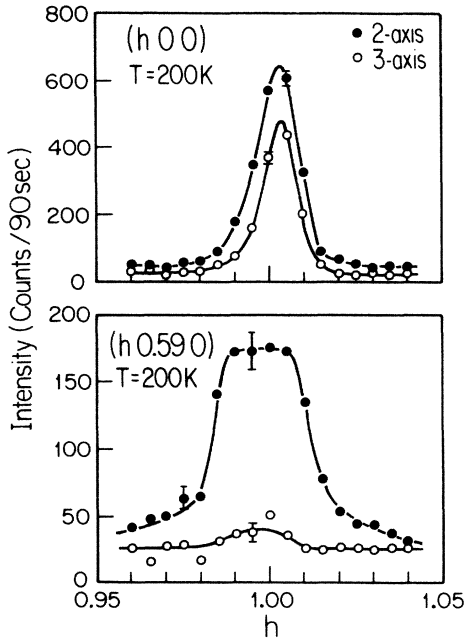


FIG. 4. Two-axis and three-axis scans across the 3D (100) magnetic peak (upper) and 2D rod (lower). The two-axis $Q$ vector corresponds to the $E=0$ position. The incoming wave vector was 2.57 Å$^{-1}$ and the collimators were 40′-10′-10′.

This large inelasticity is demonstrated in another fashion in Fig. 5. At the top of this figure is shown a two-axis scan at 300 K, again with $k_i=2.57$ Å$^{-1}$, with the in-plane wave vector $\mathbf{Q}_{2D}$ fixed at $\mathbf{a}^*$ and $\mathbf{Q}_\perp=\zeta\mathbf{b}^*$ varied. It is evident that a sharp peak occurs for $\zeta \simeq 0.6$, that is, for $\mathbf{k}_f \| -\mathbf{b}^*$. No corresponding peak occurs for $\zeta=-0.6$ so that this effect does not have the symmetry of the reciprocal lattice and hence cannot be intrinsic to $La_2CuO_4$. Thus when $k_i=2.57$ Å$^{-1}$ and $\mathbf{Q}_\perp=+0.59\mathbf{b}^*$ one measures properly the 2D correlation function $\langle S^\alpha(-\mathbf{Q}_{2D},0) \times S^\alpha(\mathbf{Q}_{2D},0)\rangle$. In general, the inelasticity involved in the 2D spin fluctuations is so large that for positions along the rod away from $\mathbf{Q}_\perp=0.59\mathbf{b}^*$, the in-plane wave vector $\mathbf{Q}_{2D}$ is varied significantly in the process of integrating over the energy thus smearing the peak and lowering the measured intensity. In order to verify the 2D nature of the scattering, a scan along the rod at 200 K was performed by use of a triple-axis spectrometer set for an energy transfer of 6 meV. The results are shown at the bottom of Fig. 5. Significant scattering occurs at $(1\zeta 0)$ whereas for $(0.9\zeta 0)$ the intensity is at the background level. As expected, the scattering for $E=6$ meV at $(1\zeta 0)$ is, except for trivial geometrical factors, independent of $\zeta$, thus confirming that these dynamic spin fluctuations are purely two dimensional in character.

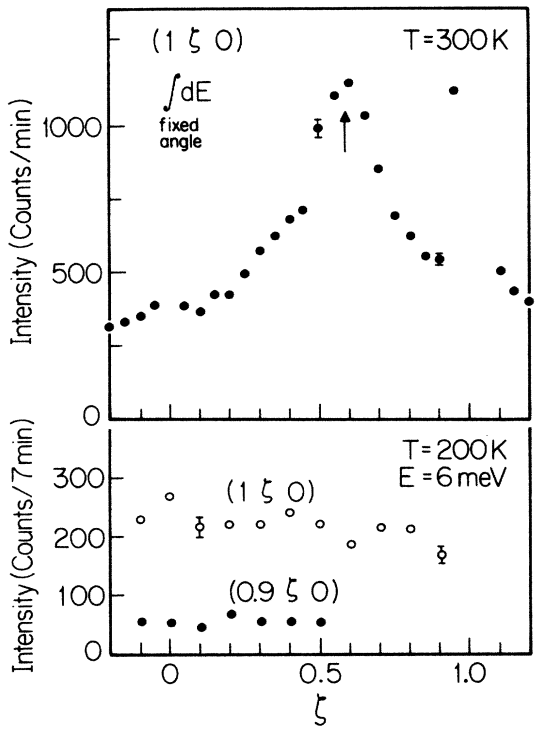


FIG. 5. Top: scan along the (1 ζ 0) rod at $T=300$ K in NTT-2. The neutron wave vector is 2.57 $Å^{-1}$. The arrow gives the position at which $\mathbf{k}_f \| -\mathbf{b}^*$ so that the energy integration for the in-plane fluctuations is carried out properly. Bottom: scans along $\mathbf{b}^*$ at a fixed energy transfer of 6 meV in NTT-2.

Even without quantitative analysis, two important qualitative features of the spin correlations in $La_2CuO_4$ may be deduced from the two-axis scan shown at the bottom of Fig. 4. First from the flat-top shape one concludes that there are equal intensity contributions from the $\mathbf{a}^*$-$\mathbf{b}^*$ and $\mathbf{c}^*$-$\mathbf{b}^*$ planes. From Eqs. (1) and (7) it follows that, at 200 K, $S^{aa}(\mathbf{Q}_{2D})=S^{cc}(\mathbf{Q}_{2D})$, that is, the fluctuations have at least $XY$ symmetry. This in turn, means that at this temperature the in-plane anisotropy[9] is not playing an important role. Second, from the sharp edges one may deduce that at 200 K the correlation length must exceed 200 Å.

The integrated intensity in the two-axis scan across the rod for NTT-2 is shown as a function of temperature at the top of Fig. 2. The rod intensity increases slightly below 300 K with decreasing temperature. However, at $T_N=195$ K the 2D scattering intensity begins to decrease. This is consistent with the heuristic notion that the 2D dynamic scattering is converted into 3D Bragg scattering at the transition to 3D long-range order (LRO). It should be emphasized, however, that in $La_2CuO_4$ this process occurs very gradually. By contrast, in $K_2NiF_4$, due to the 2D Ising nature of the transition, the transfer of intensity from the rod (which in this case is nearly elastic) to the 3D Bragg peak occurs within 2% of $T_N$.[26] This reflects a fundamental difference between the 3D phase transition in $La_2CuO_4$ and those in previously studied planar antiferromagnets. In the latter, the transitions to LRO are essentially 2D in character with the 3D ordering following parasitically.[30] In $La_2CuO_4$ the 3D coupling seems to drive the transition. As we shall discuss in more detail in Sec. VI this immediately accounts for the extreme sensitivity of the 3D moment and Néel temperature to Sr doping and to the oxygen content[7,18,19] since structural disorder will strongly influence the correlations within and between the planes and any possible transition to 3D LRO. As is evident from the panel at the top of Fig. 3, similar results are observed for NTT-3 although, as noted previously, because of macroscopic inhomogeneities, the transition is much more gradual in that crystal.

### C. Quantitative studies of the 2D instantaneous correlations

Two-axis experiments were carried out over a wide range of temperatures for all four crystals, NTT-2, NTT-3, MIT-1, and MIT-2. These experiments utilized neutrons of energy 30.5 meV; for this energy the quasielastic condition is satisfied for $\mathbf{Q}_\perp \simeq 0.4\mathbf{b}^*$. For the experiments in NTT-2 and NTT-3 the collimators were 40′-10′-10′

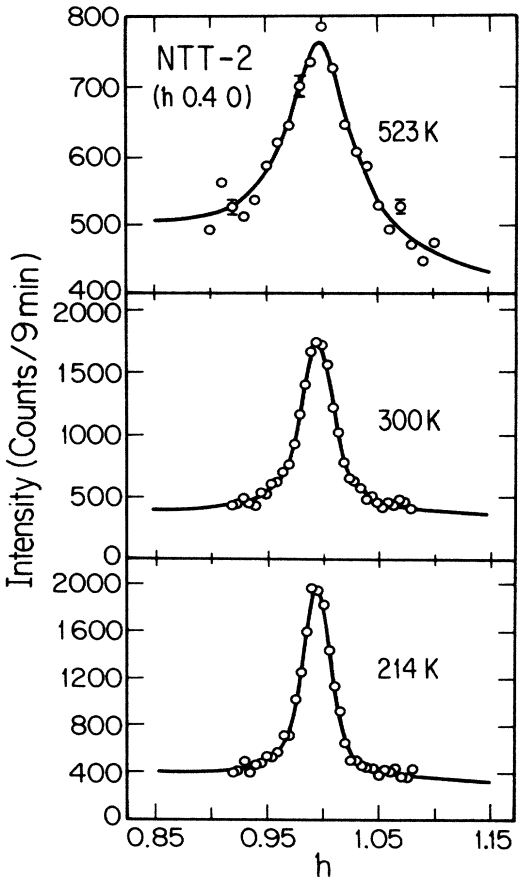


FIG. 6. Two-axis scans across the 2D rod in NTT-2 for $\mathbf{Q}_\perp=0.4\mathbf{b}^*$ at a series of temperatures. The incoming neutron energy was 30.5 meV and the collimation was 40′-10′-10′. The solid lines are the results of fits to the superposition of two Lorentzians, one centered about $\mathbf{Q}_{2D}=\mathbf{a}^*$ ($h=1$) and the other about $\mathbf{Q}_{2D}=\mathbf{c}^*$ ($h=0.993$), convoluted with the instrumental resolution function.

while for MIT-1 they were 40′-40′-40′ and for MIT-2 they were 40′-20′-40′.

Representative scans are shown in Fig. 6 for NTT-2 (as-grown $La_2CuO_4$) and in Fig. 7 for MIT-1 ($La_{1.97}Sr_{0.03}Cu_{0.95}Li_{0.05}O_4$). The flat top seen in Fig. 4 is not visible in Fig. 6 because of reduced resolution. The solid lines in Fig. 6 are the results of fits to two isotropic Lorentzians $A/(\kappa^2+q_{2D}^2)$, one centered about $\mathbf{Q}_{2D}=\mathbf{a}^*$ and one other about $\mathbf{Q}_{2D}=\mathbf{c}^*$, both convoluted with the instrumental resolution function. Here $q_{2D}=|\mathbf{Q}_{2D}-\mathbf{a}^*|$ or $|\mathbf{Q}_{2D}-\mathbf{c}^*|$; the fits also included a sloping background. The results for the inverse correlation length $\kappa$ for NTT-2 and NTT-3 (oxygenated $La_2CuO_4$) are shown individually in Fig. 8. For both crystals the correlation length evolves from about 40 Å at 500 K to about 400 Å at $T_N$. The integrated intensities, deduced from fits to a Gaussian line shape, for NTT-2 and NTT-3 are shown in Fig. 9.

The results for the inverse correlation length for all four samples are shown in Fig. 10. The empirical reason for the lack of 3D long-range order in the $Li^+$ doped samples is immediately evident. For MIT-2 the correlation length has a constant value of 40 Å below room temperature. For MIT-1, which has ~0.05 $Li^+$ and 0.03 $Sr^{2+}$ fractions, the correlation length reaches only ~20 Å at 80 K. We conclude, therefore, that the holes created by the doping with $Li^+$ and/or $Sr^{2+}$ drastically limit the growth of the 2D instantaneous correlations. Indeed, from comparison of the data in Fig. 10 for NTT-2 (as-grown) and NTT-3 (oxygenated), it is evident that even slight oxygenation measurably diminishes the 2D correlation length at a given temperature. Heuristic arguments[30] suggest that the 3D transition will occur when $kT_N \simeq J_\perp(\text{eff})\xi_{2D}^2$ where $J_\perp(\text{eff})$ is the effective between-plane coupling and $\xi_{2D}$ is the correlation length measured in units of the nearest-neighbor spacing; this yields $J_\perp(\text{eff}) \simeq 0.02$ K in $La_2CuO_4$. This drastic effect of the holes on the 2D magnetic correlations is quite remarkable. We will discuss possible models for this effect in Sec. VI.

Finally, we have also determined the maximum integrated 2D magnetic intensity for each of the four samples. The maximum intensities per unit sample volume normalized to identical spectrometer configurations for

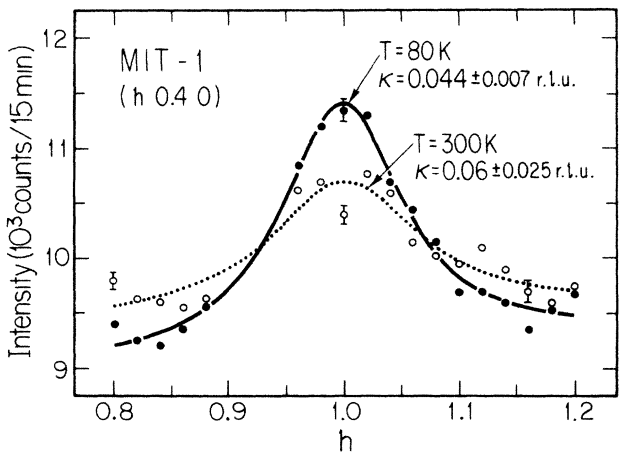


FIG. 7. Two-axis scans across the 2D rod in MIT-1 at $\mathbf{Q}_\perp=0.4\mathbf{b}^*$ at 80 and 300 K. The incoming neutron energy was 30.5 meV and the collimation was 40′-40′-40′. The solid lines are the results of fits to Lorentzians as discussed in the text. 1 r.l.u. $=2\pi/a=1.178$ Å$^{-1}$.

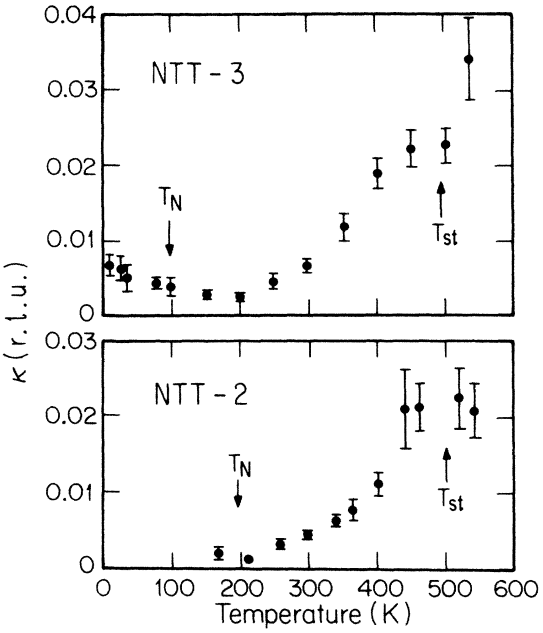


FIG. 8. Inverse correlation length vs temperature in NTT-2 and NTT-3. $T_{st}$ and $T_N$ are the structural and magnetic phase transition temperatures, respectively. The units are 1 r.l.u. $=2\pi/a=1.178$ Å$^{-1}$.

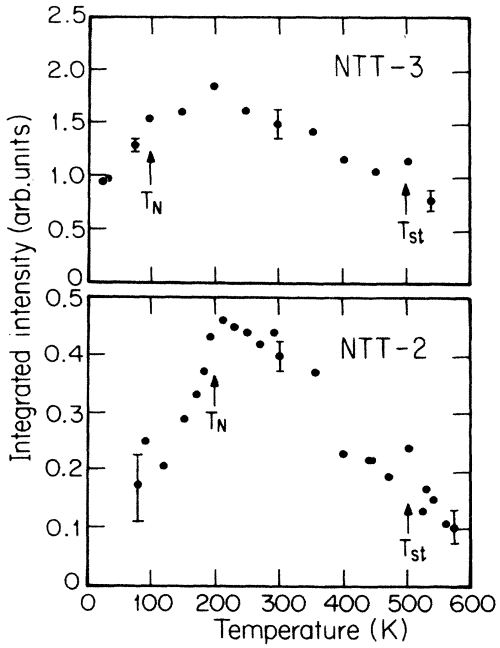


FIG. 9. Integrated intensities of the scans across the 2D rod in NTT-2 and NTT-3 as functions of temperature. $T_{st}$ and $T_N$ are the structural and antiferromagnetic transition temperatures, respectively.

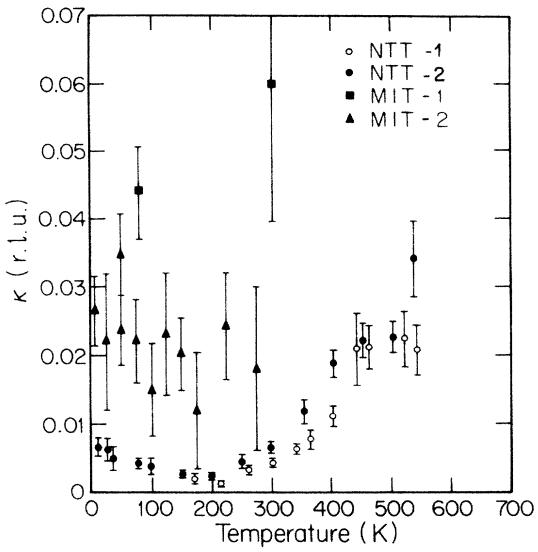


FIG. 10. Inverse correlation length vs temperature in all four samples. The units are 1 r.l.u. $=2\pi/a\simeq 1.178$ Å$^{-1}$.

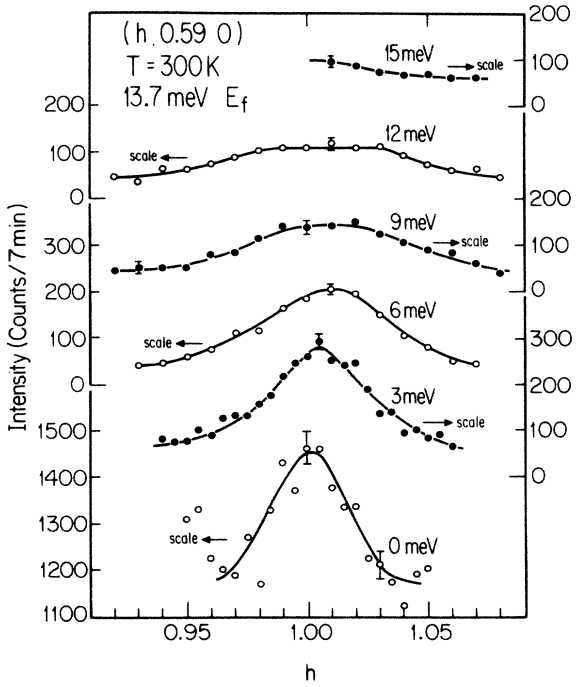


FIG. 11. Inelastic constant energy scans across the 2D rod in NTT-2 at $T=300$ K. The outgoing neutron energy was held fixed at 13.7 meV and the collimators were 40'-40'-40'-40'; here $\mathbf{Q}_{2D}=h\mathbf{a}^*$. The solid lines are guides to the eye.

NTT-2, NTT-3, MIT-1, and MIT-2 are 5.3, 4.6, 5.5, and 5.6, respectively, in arbitrary units; these numbers are accurate to about $\pm 10\%$. This is a very important result since it shows that, even though with increasing concentration of holes the magnetic correlations are drastically reduced, the net $Cu^{2+}$ moments participating in the 2D state are not changing.

## IV. INELASTIC NEUTRON-SCATTERING EXPERIMENTS

As discussed above, the quasielastic measurements in $La_2CuO_4$ indicate a large energy scale for the spin fluctuations. We have carried out a variety of inelastic measurements in order to probe the dynamics directly. Because of both sample size and magnetic correlation length limitations, meaningful data could only be obtained in the NTT-2 and NTT-3 samples. The experiments were carried out with a fixed final energy $E_f=13.7$ meV and typically with the collimator configuration 40'-40'-40'-40'. A pyrolitic graphite filter was placed after the sample in order to remove higher-order neutrons.

Because of the extremely steep slope of the excitation dispersion relation, it was necessary to carry out scans with the energy transfer fixed and the momentum transfer $\mathbf{Q}_{2D}$ varied. The results for NTT-2 and NTT-3 for $T=300$ K are shown in Figs. 11 and 12, respectively. We remind the reader that at 300 K the spin correlations are purely 2D with a correlation length of $\sim 200$ Å in both samples. For energies up to at least 12 meV the peak is centered about $\mathbf{Q}_{2D}=\mathbf{a}^*$ (or $\mathbf{c}^*$), that is $h=1$. The integrated intensity varies only gradually with increasing energy while the profile broadens progressively; this is especially noticeable at 12 meV in NTT-2.

This evolution of the profiles with increasing energy may be readily understood by an appropriate considera-

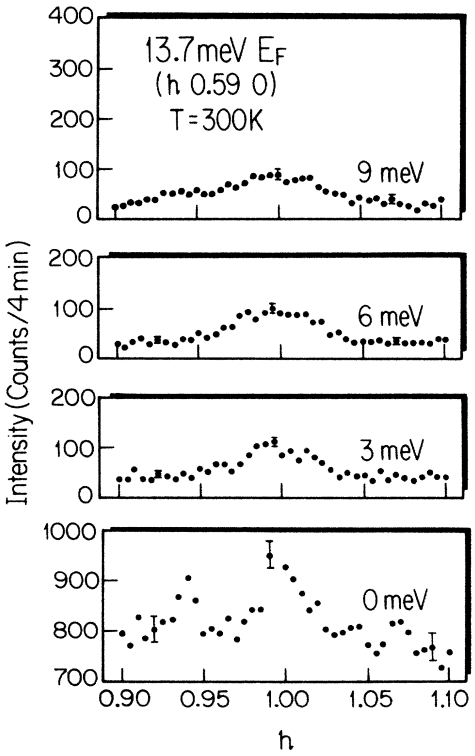


FIG. 12. Inelastic constant energy scans across the 2D rod in NTT-3 at $T=300$ K. The outgoing neutron energy was held fixed at 13.7 meV and collimators were 40'-40'-40'-40'; here $\mathbf{Q}_{2D}=h\mathbf{a}^*$.

tion of resolution effects. This is illustrated in the inset of Fig. 13. Assume for simplicity that the dynamics are described by sharp magnonlike excitations with a linear dispersion relation originating from $h=1$. If the slope of $E$ vs $|q_{2D}|$, where $q_{2D}=Q_{2D}-a^*$ or $Q_{2D}-c^*$, is steep enough, then with the energy set at, say 9 meV, it may not be possible to resolve the $-q_{2D}$ and $+q_{2D}$ branches. Figure 13 shows a calculation of the predicted profiles assuming gapless spin-wave excitations obeying Bose statistics. The line shape is taken as a Lorentzian $\Gamma/\{\Gamma^2+[\omega-\omega(q_{2D})]\}^2$ with $\Gamma=1$ meV and $\omega(q_{2D})=v|q_{2D}|$ with $v=0.34$ eV reciprocal-lattice units (r.l.u.) or 0.4 eV Å. The Lorentzian is convoluted with the instrumental resolution function. We note that the vertical $q$ resolution is 0.05 $Å^{-1}$ half width at half maximum which corresponds to an effective energy resolution of $\sim$20 meV for the above excitation velocity. As the simulation clearly shows, for a slope of 0.4 eV Å the $-|q_{2D}|$ and $|q_{2D}|$ excitations could not have been resolved. From the experimental profiles we estimate that the excitation velocity is $\gtrsim$0.4 eV Å; however, velocities as large as twice this value cannot be excluded.[31] As one might expect, the calculated intensities diverge as $E$ decreases towards zero due to the fact that the calculation assumes Bose statistics. This clearly disagrees with the experiments. Indeed, as observed indirectly in the quasielastic experiments, there is very little weight in the excitations at low energies. We have carried out simulations assuming both Bose and Fermi statistics; the experiment does not choose between these two. However, the assumption of sharp excitations at 300 K may itself not be correct, so assigning statistics to the excitations may have no meaning.

In the bottom panel of Fig. 14 we show the $E=3$ meV scan in NTT-2 ($T_N\simeq 195$ K) as a function of temperature between 5 and 300 K. The peak intensity versus temperature is shown in the top panel. The intensity is approximately independent of temperature between 300 and $\sim$150 K and drops off considerably in intensity below 150 K. From 5 up to 150 K the intensity follows the Bose

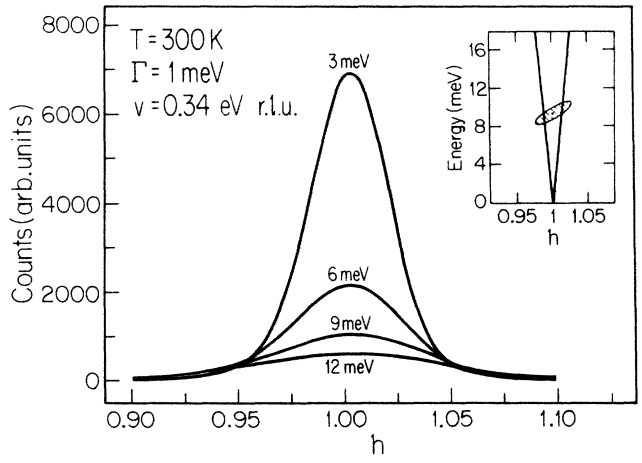


FIG. 13. Simulation of the constant energy scans in Figs. 11 and 12 assuming simple Bose spin waves with velocity $v=0.34$ eV r.l.u. and an energy width $\Gamma=1$ meV. The inset illustrates the size of the instrumental resolution function relative to the spread in $h$ of the excitations. 1 r.l.u. $=2\pi/a=1.178$ $Å^{-1}$.

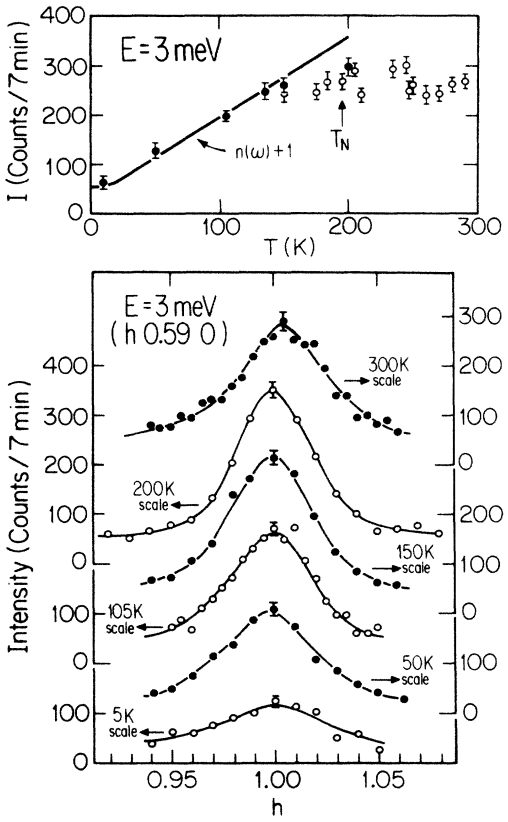


FIG. 14. Top: integrated intensity of the $E=3$ meV constant energy scans vs temperature. $T_N$ is the Néel temperature in this sample. The solid line is the prediction for the temperature dependence of the intensity assuming Bose statistics $E=(e^{\hbar\omega/kT}-1)^{-1}+1$. Bottom: constant energy scans at $E=3$ meV in NTT-2. The outgoing neutron energy is 13.7 meV and the collimation 40'-40'-40'-40'.

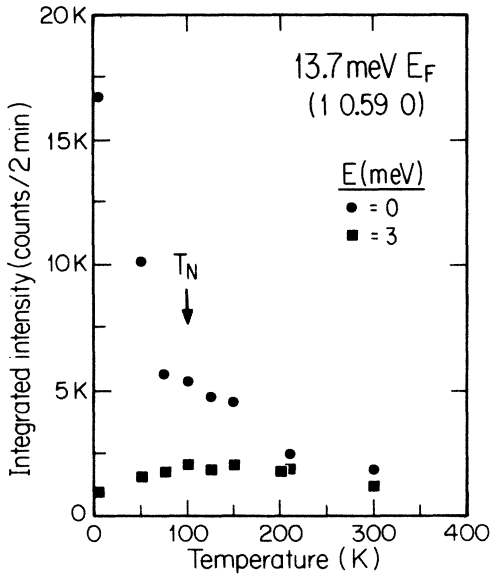


FIG. 15. Integrated intensity of constant energy scans vs temperature at 0 and 3 meV in NTT-3. $T_N$ is the Néel temperature. The outgoing neutron energy was held fixed at 13.7 meV and the collimation was 40'-40'-40'-40'.

statistics curve quite well. We conclude, therefore, that the quantum spin fluid spin excitations become simple spin waves in the Néel state, as one might have expected.

In Fig. 15 we show the integrated intensity in NTT-3 ($T_N \simeq 100$ K) at energy transfers of 0 and 3 meV. The behavior at 3 meV is closely similar to that in NTT-2. For $E=0$ the intensity increases gradually through $T_N$ and rises dramatically at low temperatures. This rapid rise of the 2D quasielastic scattering at low temperatures mirrors the reentrant diminution of the 3D Bragg intensity as shown in Fig. 3. As discussed in Sec. VI this may be interpreted as indicating reentrant spin-glass behavior.[11,27]

Finally, the low-energy excitations in NTT-2 at 80 K have been studied by Peters *et al.*[9] They find in the Néel state energy gaps of $1.0 \pm 0.25$ meV and $2.5 \pm 0.5$ meV for motion of the spins, respectively, in and out of the a-c plane. They also observe an increase in the scattering at $E=0$ at low temperatures similar to that shown for NTT-3 in Fig. 15 but of much smaller magnitude.

## V. POLARIZED NEUTRON MEASUREMENTS

We have also carried out some limited measurements of the spin dynamics using polarized neutron techniques. Such measurements are very time consuming because of the loss in intensity due to the polarizing crystals and because of the selection of a single spin component. Thus we only did measurements at one representative energy transfer 3 meV at selected temperatures above and below $T_N$. The incoming energy was fixed at 44 meV and the outgoing energy at 41 meV. The collimation was 40'-80'-80'-130' and the consequent energy resolution was 7 meV full width at half maximum. The instrumental polarization was of high enough quality that the flipping ratio was better than 16. There are two basic polarization modes: non-spin-flip (NSF) and spin-flip (SF). In addition the neutron polarization may be chosen to be either parallel to the scattering vector Q or perpendicular to the scattering plane. These are achieved by having the magnetic field around the sample either along Q (HF) or in the vertical direction (VF) perpendicular to the scattering plane and thus Q.

A particularly simple result holds if one takes appropriate differences. Specifically, one predicts for the magnetic scattering

$$I_{\mathrm{NSF}}(\mathrm{VF}) - I_{\mathrm{NSF}}(\mathrm{HF}) = I_{\mathrm{SF}}(\mathrm{HF}) - I_{\mathrm{SF}}(\mathrm{VF}) = S^{V}(\mathbf{Q},\omega) \ , \tag{6}$$

when $S^{V}(\mathbf{Q},\omega)$ is the component in the vertical direction perpendicular to the scattering plane. In this case because of the twin domains $S^{V}(\mathbf{Q},\omega) = \frac{1}{2} S^{\mathrm{a,a}} + \frac{1}{2} S^{\mathrm{c,c}}$. As shown at the top of Fig. 16, at 200 K the NSF and SF intensity differences at (1 0.59 0) (far away from the 3D Bragg peak) are essentially the same. This confirms unambiguously that the 2D scattering is indeed magnetic as assumed in Sec. III and Sec. IV. As shown in the bottom panel of Fig. 16 the spin-flip cross section decreases significantly in intensity in going from above to below $T_N = 195$ K. This is consistent with the crossover from isotropic quantum spin fluid excitations to spin waves inferred in Sec. IV.

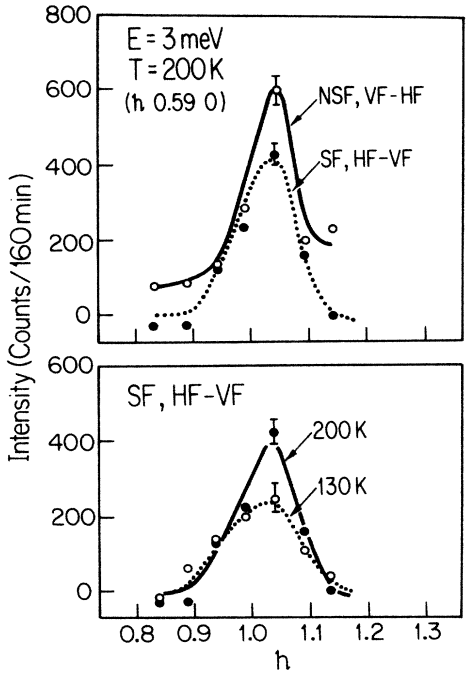


FIG. 16. Top: polarized neutron scans at 200 K in NTT-2 for $E=3$ meV. Bottom: spin-flip HF-VF cross section at 3 meV energy transfer at 200 and 130 K. The collimation was 40'-80'-80'-130'.

## VI. DISCUSSION AND CONCLUSIONS

These experiments have revealed a variety of interesting features in the static and dynamic spin correlations in pure and doped $La_2CuO_4$. The magnetic behavior in these systems is dominated by the 2D $CuO_2$ planes. The spin Hamiltonian describing the stoichiometric material is very close to that of the idealized 2D, $S=\frac{1}{2}$ Heisenberg model

$$H = \sum_{\substack{i,j \\ i>j}} J_{ij} \mathbf{S}_i \cdot \mathbf{S}_j \ . \tag{7}$$

If we assume nearest-neighbor interactions alone, the exchange interaction $J_{\mathrm{NN}}$ is $\geq 850$ K. The anisotropy energies for motion of the spins out of the a-c plane is $\sim 0.1$ K while the effective interplanar coupling is $J_{\perp}(\mathrm{eff}) \simeq 0.02$ K. As discussed by Thio *et al.*[7] the largest correction to the Heisenberg Hamiltonian is the antisymmetric exchange energy of 1.1 meV generated by the rotation of the $CuO_6$ octahedra.

Quantum effects clearly play a fundamental role. First, the fluctuations in the 2D state above $T_N$ are highly inelastic with no significant quasielastic component even very near $T_N$. This is in marked contrast to the critical dynamics in other 2D and 3D antiferromagnets even including itinerant systems such as $Cr_{0.95}Mn_{0.5}$ (Ref. 32) where the quasielastic component dominates near $T_N$. The latter behavior is consistent with the critical slowing down expected as the correlation length becomes very large. The behavior in $La_2CuO_4$ is much more akin to that in the 1D $S=\frac{1}{2}$ Heisenberg antiferromagnet at $T=0$ where the fluctuations at a given $q$ are bounded in energy below by $\pi J \sin(qa)$.[29,33] Second, as emphasized

in Ref. 34 the actual correlation length itself is strongly influenced by quantum fluctuations. For a classical 2D Heisenberg model the correlation length[35] is

$$\xi/a = e^{2\pi JS^2/kT} . \quad (8)$$

If we replace $JS^2$ by $JS(S+1) \simeq 650$ K then at 300 K one estimates $\xi/a \simeq 8\times10^5$. That is, the correlation length for classical spins would already be macroscopic at room temperature; this disagrees by 4 orders of magnitude with our result in $La_2CuO_4$ at 300 K, $\xi/a \simeq 50$. In an elegant recent paper Chakravarty, Halperin, and Nelson[34] have shown that the quantum corrections to Eq. (8) bring the theory into very good agreement with our experiments for NTT-2 over the complete range of temperature above $T_N$ from 200 to 550 K.

The 2D and 3D magnetic states in $La_2CuO_4$ are remarkably sensitive to doping.[7,18,19] This is illustrated most clearly in Fig. 10. First, the oxygenation of the as-grown $La_2CuO_4$ crystal reduces $T_N$ from 195 K to $\sim$100 K due to a suppression of the in plane correlations. The addition of $\sim$5% $Li^+$ eliminates the 3D transition completely and reduces the low-temperature 2D correlation length to 40 Å. This is most certainly not due to the simple removal of 5% of the Cu spins since extensive studies of diluted 2D magnets show such dilution is benign as long as one is not near the percolation threshold.[36] The effect rather originates from the 5% concentration of holes created by the $Li^+$ doping in order to maintain charge neutrality. By analogy with experiments on $Sr^{2+}$ doping, we expect the holes to be localized on the in-plane oxygens.[37] However, in contrast to the Sr-doped samples the presence of the $Li^+$ in the $CuO_2$ planes localizes the holes thus producing variable range hopping rather than metallic conductivity behavior. The $Li^+$ therefore also suppresses the superconductivity. We expect, however, that the effect of the holes on the magnetism is similar whether the doping is by $Li^+$ replacing $Cu^{2+}$ or $Sr^{2+}$ replacing $La^{3+}$. This view is reinforced by the results in MIT-1; they show that the increase in the number of holes from $\sim$5% to $\sim$8%, by the addition of 0.03 $Sr^{2+}$, reduces the limiting correlation length from $\sim$40 Å in MIT-2 to $\sim$20 Å in MIT-1. We believe that the magnetism in these samples is likely to be closely similar to that in samples doped with $Sr^{2+}$ alone and which therefore would be metallic at 300 K and superconducting at low temperatures. Of course, experiments on the appropriate samples must be performed to establish this definitely.

As discussed by Aharony *et al.*,[11] a number of basic features of the magnetism may be understood using a simple classical model. They begin with the 3D Néel state at low temperatures, which they treat in a classical approximation. The hole (spin $\sigma$) is presumed to reside on an in-plane oxygen and to be strongly coupled to the surrounding $Cu^{2+}$ spins so that $H = J_\sigma \sigma \cdot [\mathbf{S}_1(Cu^{2+}) + \mathbf{S}_2(Cu^{2+})]$. The ground state, which is at energy $-J_\sigma$ for these three spins, is either a doublet $\sqrt{2/3}|+-+\rangle - \sqrt{1/6}|++-\rangle - \sqrt{1/6}|-++\rangle$ or the $|+++\rangle$ quartet. For the doublet Aharony *et al.*[11] then project out the major component, $|+-+\rangle$, which is, in fact, the classical ground state. The two $Cu^{2+}$ spins surrounding an $O^-$ hole are thus ferromagnetically aligned and this frustrates the presumed ideally ordered Néel state. Thus the phase diagram is that of a quasi-2D spin system with competing antiferromagnetic and ferromagnetic interactions. As discussed by Aharony *et al.*,[11] the basic features of the magnetic phase diagram can be readily understood using this model. Specifically the model suggests that in NTT-3 the diminution of the Bragg peak and the appearance of intense $E \simeq 0$ 2D diffuse scattering signal reentrant spin-glass behavior. There is also a long-range $1/R^2$ oscillatory coupling between the holes through the $Cu^{2+}$ spin system. The relevance of this coupling to the superconductivity is discussed in Ref. 38.

In conclusion, pure and doped $La_2CuO_4$ show very interesting magnetic behavior. The pure system is very close to being an ideal realization of the 2D $S = \frac{1}{2}$ square-lattice Heisenberg model, a problem of fundamental interest in statistical physics. Our experiments have already stimulated some new, promising theories on this problem,[34,39] although much work remains to be done, especially on the dynamics. The energy scale for the spin fluctuations in the $CuO_2$ plane is quite large; corresponding to magnetic excitation velocities ten times the speed of sound in the material. Of course, this large energy scale is one essential ingredient in theories of the superconductivity which rest on magnetic coupling mechanisms.

The experiments on doped samples show that the holes seriously inhibit the development of the 2D correlations. We infer that the spins in superconducting samples will only be correlated over short distances although this remains to be proven experimentally. One may, however, make one strong statement about possible theories for the superconductivity. The experiments show that the individual $Cu^{2+}$ spins themselves are not affected by the doping since the integrated intensity remains constant. However, the carriers are strongly coupled to the $Cu^{2+}$ spins. Thus any theory for the superconductivity in doped $La_2CuO_4$ (and presumably $YBa_2Cu_3O_{6+y}$) must take into account the fact that the host lattice contains a concentrated, rapidly fluctuating spin system strongly coupled to the carriers. It is difficult to see how any theory based on a non-magnetic mechanism for the superconductivity can satisfy this requirement.

## ACKNOWLEDGMENTS

We have enjoyed many stimulating discussions of this work with a variety of people including G. Aeppli, A. Aharony, J. Als-Nielsen, P. W. Anderson, J. D. Axe, M. R. Beasley, W. R. Brinkman, S. Chakravarty, A. Coniglio, V. J. Emery, B. I. Halperin, P. M. Horn, A. Kapatulnik, R. B. Laughlin, P. A. Lee, D. E. Moncton, D. R. Nelson, J. Orenstein, T. M. Rice, J. R. Schrieffer, J. P. Sethna, S. K. Sinha, H. E. Stanley, M. Strongin, and Y. J. Uemura. This work was supported by the U.S.-Japan Cooperative Neutron Scattering Program, and a Grant-in-Aid for Scientific Research from the Japanese Ministry of Education, Science, and Culture. The work at MIT was supported by the National Science Foundation under Contracts No. DMR85-01856 and No. DMR84-18718. Research at Brookhaven is supported by the Division of Materials Science, U.S. Department of Energy under Contract No. DE-ACO2-CH00016.

[1]J. G. Bednorz and K. A. Müller, Z. Phys. B **64**, 189 (1986).
[2]V. B. Grande, Hk. Müller-Buschbaum, and M. Schweizer, Z. Anorg. Allg. Chem. **428**, 120 (1977).
[3]R. J. Birgeneau, C. Y. Chen, D. R. Gabbe, H. P. Jenssen, M. A. Kastner, C. J. Peters, P. J. Picone, Tineke Thio, T. R. Thurston, H. L. Tuller, J. D. Axe, P. Boni, and G. Shirane, Phys. Rev. Lett. **59**, 1329 (1987).
[4]M. Onoda, S. Shamoto, M. Sato, and S. Hosoya, Jpn. J. Appl. Phys. **26**, L363 (1987).
[5]R. M. Fleming, B. Batlogg, R. J. Cava, and E. A. Rietman, Phys. Rev. B **35**, 7191 (1987); R. B. van Dover, R. J. Cava, B. Batlogg, and E. A. Rietman, *ibid.* B **35**, 5337 (1987).
[6]D. Vaknin, S. K. Sinha, D. E. Moncton, D. C. Johnston, J. M. Newsom, C. R. Safinya, and H. E. King, Jr., Phys. Rev. Lett. **58**, 2802 (1987).
[7]K. Yamada, E. Kudo, Y. Endoh, Y. Hidaka, M. Oda, M. Suzuki, and T. Murakami, Solid State Commun. **64**, 753 (1987); Tineke Thio, T. R. Thurston, N. W. Preyer, P. J. Picone, M. A. Kastner, H. P. Jenssen, D. R. Gabbe, C-Y. Chen, R. J. Birgeneau, and Amnon Aharony, Phys. Rev. B (to be published).
[8]G. Shirane, Y. Endoh, R. J. Birgeneau, M. A. Kastner, Y. Hidaka, M. Oda, M. Suzuki, and T. Murakami, Phys. Rev. Lett. **59**, 1613 (1987).
[9]C. J. Peters, R. J. Birgeneau, M. A. Kastner, H. Yoshizawa, Y. Endoh, J. Tranquada, G. Shirane, Y. Hidaka, M. Oda, M. Suzuki, and T. Murakami, Phys. Rev. B (to be published).
[10]D. Harshman *et al.* (unpublished); Y. J. Uemura (private communication); Y. J. Uemura *et al.*, Phys. Rev. Lett. **59**, 1045 (1987).
[11]A. Aharony, R. J. Birgeneau, A. Coniglio, M. A. Kastner, and H. E. Stanley, Phys. Rev. Lett. **60**, 1330 (1988).
[12]M. A. Kastner, R. J. Birgeneau, C. Y. Chen, Y. M. Chiang, D. R. Gabbe, H. P. Jensen, T. Junk, C. J. Peters, P. J. Picone, Tineke Thio, T. R. Thurston, and H. L. Tuller, Phys. Rev. B **37**, 111 (1988).
[13]See, for example, P. W. Anderson, Science **235**, 1196 (1987); P. W. Anderson, G. Baskaran, Z. Zou, and T. Hsu, Phys. Rev. Lett. **58**, 2790 (1987); V. J. Emery, *ibid.* **58**, 2794 (1987); P. A. Lee and M. Read, *ibid.* **58**, 2691 (1987); J. E. Hirsch, *ibid.* **59**, 228 (1987); S. A. Kivelson, D. S. Rokhsar, and J. P. Sethna, Phys. Rev. B **35**, 8865 (1987); C. Gros, R. Joynt, and T. M. Rice, Z. Phys. B **68**, 425 (1987); D. J. Thouless, Phys. Rev. B **36**, 7187 (1987).
[14]P. J. Picone, H. P. Jenssen, and D. R. Gabbe, J. Cryst. Growth **85**, 576 (1987).
[15]Y. Hidaka, Y. Enomoto, M. Suzuki, M. Oda, and T. Murakami, Jpn. J. Appl. Phys. **26**, L377 (1987); J. Cryst. Growth **85**, 581 (1987).
[16]D. Balz and K. Pleith, Z. Elektrochem. **59**, 545 (1955).
[17]J. D. Jorgensen, H. B. Schusttler, D. G. Hinks, D. W. Capone II, K. Zheng, M. Brodsky, and D. J. Scalapino, Phys. Rev. Lett. **58**, 1024 (1987).
[18]D. C. Johnston, J. P. Stokes, D. P. Goshorn, and J. T. Lewandowski, Phys. Rev. B **36**, 4007 (1987).
[19]T. Freltoft, J. P. Remeika, D. E. Moncton, A. S. Cooper, J. E. Fischer, D. Harshman, G. Shirane, S. K. Sinha, and D. Vaknin, Phys. Rev. B **36**, 826 (1987).
[20]J. M. Delgado, R. K. McMullan, G. Díaz de Delgado, B. J. Wuensch, P. J. Picone, H. P. Jennsen, and D. R. Gabbe, Phys. Rev. B (to be published).
[21]N. F. Mott and E. A. Davis, *Electronic Processes in Non-Crystalline Materials,* 2nd ed. (Clarendon, Oxford, 1979).
[22]V. Ambegaokar, B. I. Halperin, and J. S. Langer, Phys. Rev. B **4**, 2612 (1971).
[23]P. M. Grant, S. S. Parkin, Y. Y. Lee, E. M. Engler, M. L. Ramirez, J. E. Vazquez, G. Lim, R. D. Jacowitz, and R. L. Greene, Phys. Rev. Lett. **58**, 2482 (1987); J. Beille, R. Cabanel, C. Chaillout, B. Chevallier, G. Demazeau, F. Deslandes, J. Etourneau, P. Lejay, C. Michel, J. Provost, B. Raveau, A. Sulpice, J-L. Tholence, and R. Tournier, Z. Phys. B (to be published).
[24]W. Marshall and R. Lowde, Rep. Prog. Phys. **31**, 705 (1968).
[25]R. J. Birgeneau, J. Skalyo, Jr., and G. Shirane, Phys. Rev. B **3**, 1736 (1971).
[26]R. J. Birgeneau, J. Als-Nielsen, and G. Shirane, Phys. Rev. B **16**, 280 (1977).
[27]For a review of similar experiments on $Eu_xSr_{1-x}S$ and $(Fe_xMn_{1-x})_{75}P_{16}B_6Al_3$, see G. Aeppli, S. M. Shaprio, H. Maletta, R. J. Birgeneau, and H. S. Chen, J. Appl. Phys. **55**, 1628 (1984).
[28]See, for example, P. W. Anderson, Mater. Res. Bull. **8**, 153 (1973).
[29]Y. Endoh, G. Shirane, R. J. Birgeneau, P. M. Richards, and S. L. Holt, Phys. Rev. Lett. **26**, 718 (1973); I. A. Heilmann, G. Shirane, Y. Endoh, R. J. Birgeneau, and S. L. Holt, Phys. Rev. B **19**, 3530 (1978).
[30]R. J. Birgeneau, G. Shirane, and H. J. Guggenheim, Phys. Rev. Lett. **22**, 720 (1969); Phys. Rev. B **1**, 2211 (1970); R. J. Birgeneau, J. Skalyo, Jr., and G. Shirane, J. Appl. Phys. **41**, 1303 (1970).
[31]K. P. Lyons, P. A. Fleury, J. P. Remeika, A. S. Cooper, and T. J. Negran, Phys. Rev. B **37**, 2393 (1988). From the two-magnon Raman profile these authors deduce a value of the spin-wave velocity of $\sim 0.7$ eV Å corresponding to an exchange $J_{NN} = 116$ meV.
[32]J. Als-Nielsen, J. D. Axe, and G. Shirane, J. Appl. Phys. **42**, 1666 (1971).
[33]J. J. des Cloizeaux and J. J. Pearson, Phys. Rev. **128**, 2131 (1962); J. C. Bonner and B. Sutherland, in *Magnetism and Magnetic Materials—1974,* Proceedings of the 20th Annual Conference on Magnetism and Magnetic Materials, AIP Conference Proceedings No. 24, edited by C. D. Graham, G. H. Lander, and J. J. Rhyne (AIP, New York, 1975), p. 355; H. J. Mikeska, Phys. Rev. B **12**, 7 (1975); **12**, 2794 (1975).
[34]S. Chakravarty, B. I. Halperin, and D. R. Nelson, Phys. Rev. Lett. **60**, 1057 (1988).
[35]A. M. Polyakov, Phys. Lett. B **59**, 79 (1975); D. R. Nelson and R. A. Pelcovitz, Phys. Rev. B **16**, 2191 (1977).
[36]R. J. Birgeneau, R. A. Cowley, G. Shirane, J. A. Tarvin, and H. J. Guggenheim, Phys. Rev. B **21**, 317 (1980); R. A. Cowley, R. J. Birgeneau, G. Shirane, H. J. Guggenheim, and H. Ikeda, *ibid.* **21**, 4038 (1980); H. Ikeda, J. Phys. Soc. Jpn. **50**, 3215 (1981), and references therein.
[37]J. M. Tranquada, S. L. Heald, and A. R. Moodenbaugh, Phys. Rev. B **36**, 5263 (1987).
[38]R. J. Birgeneau, M. A. Kastner, and A. Aharony, Z. Phys. B (to be published).
[39]P. W. Anderson, Phys. Rev. Lett. **59**, 2497 (1987); I. Affleck (unpublished).